

Experimental analysis of solid-propellant surface during combustion with shadowgraphy images: new tools to assist aluminum-agglomeration modelling

Robin William Devillers*, Guy Le Besnerais**, Matthieu Nugue*, Nathalie Cesco***

*ONERA, Fundamental & Applied Energetics Department

BP 80100 – 91123 Palaiseau Cedex France, Email: robin.devillers@onera.fr

**ONERA, [System](#) & Information Processing Department

BP 80100 – 91123 Palaiseau Cedex France, Email: guy.le_besnerais@onera.fr

***CNES, The Launcher Directorate

52 rue Jacques Hillairet – 75612 Paris Cedex France, Email: nathalie.cesco@cnes.fr

Abstract

Studying two-phase flow in solid-propellant motors requires good knowledge of the initial aluminum-droplet size distribution. Droplet size is strongly influenced by agglomeration phenomena whose models need improvements. To support new developments, present work shows analysis of propellant surface phenomena on shadowgraphy images. An active contour method provides accurate surface detection whereas multi-scale surface-curvature criteria enable selecting portions of interest and follow them over time. The method is demonstrated with 4 solid-propellant compositions (3 seeded with inert particles, 1 with aluminum) burned between 1.0 and 3.0 MPa. It shows good detection performances and provides first results on size and lifetime for the detected agglomeration shapes.

1. Introduction

Solid propellants are commonly used for space and military applications due to their efficiency and low cost. Usually, powder-like oxidizers such as ammonium perchlorate (AP) are gathered into a polymer binder, for instance hydroxyl-terminated polybutadiene (HTPB). Aluminum is a usual performance additive included in the grain in order to improve and adjust effective impulse, with mass fractions up to 20%. However, in spite of the effects on temperature increase and performance benefits, the combustion of aluminum droplets can have a dramatic impact on performance stability [1][2][3], with a strong aluminum-size dependence on the stable or unstable behavior. Hence, it is crucial to have a clear knowledge of the diameter for the droplets that effectively leave the burning surface to enter the rocket flow, but such a knowledge is not as straightforward as it seems: the aluminum droplets leaving the surface usually result from the agglomeration of various aluminum particles that had initially been seeded into the energetic material.

Various approaches have been taken in order to model the aluminum-agglomeration phenomena, first with correlations based on sampled alumina residues or other experimental data [4][5][6][7], on pocket-like models [8][9], and more recently on statistical analysis of simulated materials made of random spheres [10][11][12]. Still, the detailed physical phenomena taking place on the surface during combustion need to be accurately described, such as the governing factors for a short or a long aluminum residence time on the propellant surface. This involves accurate experimental data for the surface during combustion that would be representative of real propellant-combustion conditions with sufficient time resolution. But such data remain scarce and with limited statistic and quantitative results regarding the propellant surface itself [13][14][15].

In order to provide better experimental data sets for solid-propellant combustion, a focusing shadowgraphy set-up has been in use at ONERA to enable aluminum-particle visualization at high repetition rate close to the surface of burning propellant samples [16][17][18]. The experimental images have been processed in previous studies via various image analysis methods in order to provide particle size distribution [17][18] or velocity profiles for burning droplets ejected from the surface into combustion gases [17]. But surface phenomena have not been analyzed in details so far in spite of the images potential to provide insights on agglomeration phenomena or surface residence time. In the present work, recent image analysis methods are used for a better characterization of the burning surface as well as the detection of time-resolved aluminum-agglomeration phenomena. The method is demonstrated for a

range of experimental conditions obtained by burning four solid-propellant compositions seeded with inert particles or aluminum, burned for operating pressures between 1.0 and 3.0 MPa.

2. Experimental work

2.1. Shadowgraphy set-up

The present solid-propellant study is performed in a high-pressure chamber with optical windows enabling combustion visualization. Propellant samples are small, usually below 0.5 g for each test, since the area of study remains close to the propellant surface. The chamber is initially pressurized with pure nitrogen, from 1.0 to 4.0 MPa. Solid propellant samples are ignited via a CO₂-laser beam entering the chamber via a window on top. The experimental imaging of propellant combustion stems from a focused shadowgraphy set-up [19] illustrated in Figure 1, whose application for solid-propellant study has been described previously [16][17]. Broadband light is focused through the combustion area in order to provide intense lighting even compared to bright solid-propellant flames; focalization also aims at working with reduced depth of field, limiting particle density on the images. The image collection set-up works as a close-up optical apparatus enabling visualization of single particles down to around 10 μm in diameter, which is an interesting range considering aluminum-particle size common for AP/HTPB composite propellants. High-speed camera is used above 1 kHz-repetition rates so that aluminum particles and physical phenomena on the surfaces can be followed in time on successive images.

Figure 1 also shows a typical shadowgraphy image acquired during combustion of solid propellants seeded with aluminum particles. Two regions appear clearly: the solid propellant in dark at the bottom, and the hot-gas zone above in brighter gray. The gas area is a result of propellant combustion and is populated with burning aluminum droplets (visible as bright objects on the image) as well as still-inert aluminum that left the propellant surface before their ignition (visible as dark single objects). Smoke is also visible in the background of the gas area. The solid propellant area at the bottom appears much more homogeneous but its surface often shows complex shapes and patterns. Most of surface protruding objects usually correspond to phenomena associated to aluminum particles: aluminum melting on the surface, aluminum ignition, agglomeration of various aluminum droplets, ejection from the surface... Present work aims at focusing on surface analysis in order to detect such phenomena, which can be difficult depending on the image conditions. High-pressure conditions, large objects density on the pictures, high noise associated to low light level usually make it difficult to apply automatic detection methods efficiently and robustly. This will be the goal of the present work.

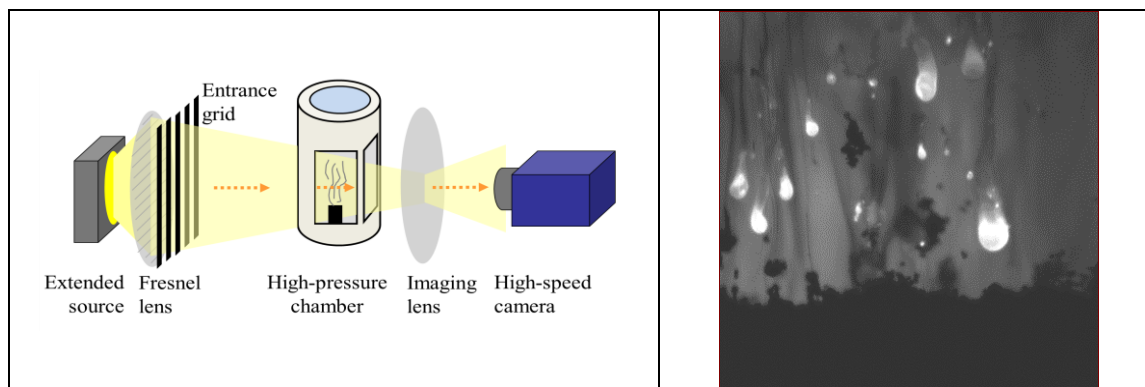


Figure 1. Shadowgraphy set-up and typical image for aluminum-seeded solid propellant combustion.

2.2. Propellants and burning conditions

Four solid propellant compositions have been studied in combustion in order to evaluate the capacity of the present surface analysis under conditions of increasing complexity. All of them are AP/HTPB composite propellants with usual proportions; hence close enough to real-application propellants. Three of them were seeded with inert particles, leading to more favorable image analysis; the last composition was seeded with aluminum particles and is similar to common industrial propellants.

The three propellants seeded with inert particles contained around 6% mass fraction of such particles. The low particle fraction leads to low particle density in the burning gases above the propellant surface, which is ideal to

segment the remaining propellant via automatic analysis. This provided a baseline for the surface analysis: an analysis method that would face high difficulties dealing with propellant surface in such conditions would not be worth investigating much further for more stringent conditions. Each of the three compositions was seeded with a different kind of material with specific size range; the various diameter intervals are illustrated in Figure 2. The first composition, labeled “glass composition”, was seeded with zircon oxide particles ranging from 6 to 120 μm in two narrow probability peaks (e.g. binomial distribution); the most visible particles had diameter between 53 to 133 μm clearly visible on the shadowgraphy images. The second composition was seeded with titanium oxide, which does not burn at the pressure conditions tested here. The diameter of the single particles ranged from 57 to 75 μm , smaller than the main particles from the glass compositions. The last inert composition was seeded with magnesium oxide particles in the range of 5 to 17 μm in diameter.

The more realistic propellant was seeded with 18% mass fraction of aluminum particles, which is an usual mass fraction range for industrial composite propellants. The size distributions ranged from 15 to 160 μm diameter with a probability peak around 65 μm . This is a fairly wide distribution but the diagnostic spatial resolution is sufficient to visualize clearly all particles present on the images. The aluminum propellant should provide a glimpse of the image analysis challenges faced when studying industrial aluminized propellant, such as combustion at the surface, bright burning aluminum droplets, alumina smoke darkening the gas area... The characteristics of the four propellant compositions are gathered in Table 1. The table also includes the main characteristics of the associated shadowgraphy images, which are commented in the next paragraph.

Table 1 Image conditions for the various image series.

label	Seeded particles	Diameter range (μm)	Surface aspect	Pressure (MPa)	Gas-area aspect
Glass		6 ; 21 53 ; 133	Largely plane and regular Some snowman-like aggregates	1.0	Very homogenous
				3.0	Small vertical smoke patterns
Ti	TiO ₂	57 ; 75	Regular surface with significant number of caterpillar-like aggregates	1.0	Very homogeneous
Mg	MgO	5 ; 17	More complex surface, with small and large snowflake-like aggregates	1.0	Homogeneous, with numerous small particles
Al	Al	15 ; 160	Complex surface, with various size of aggregates	2.0	Dark and bright particles and vertical smoke lead to less homogeneous area
				3.0	Very heterogeneous area with large density of object (burning particles, smoke)

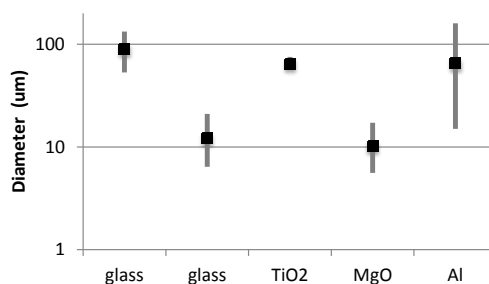


Figure 2. Diameter range for particles seeded into the tested solid-propellant compositions.

2.3. Image characteristics for the analyzed data

As presented above, the choice of dealing with various propellant compositions was motivated by the idea of applying the surface analysis to data with different characteristics. In addition to the mere composition, various operating pressures were tested between 1.0 to 3.0 MPa: the larger the pressure, the denser the object population in the gas area above the propellant surface, hence the less homogeneous the area that needs to be separated from the burning propellant area. Moreover, the difference in particle size interval leads to different aggregate aspects: for

instance, the much smaller MgO particles are expected to lead to snowflake-like aggregates and surface patterns with smaller features for propellant “Mg”. Six images series have been considered in total.

In order to be more systematic in studying the analysis performance, images were characterized with four parameters, summed up in Table 2. First, a contrast *Cont* was introduced as the signal difference between the gas area and the solid propellant area, quantified from the two averaged values; images with low contrasts between the two areas will be prone to larger surface-segmentation uncertainty. Second, the gradient at the border *Grad* is also important: smooth transition on the image from the dark surface to the clear gas area will lead to uncertain border definition. Third, the homogeneity of the flame area *Hom* is a potential source of errors. A clear homogeneous gas zone will be easy to isolate whereas crowded smoky zones might lead to false alarm, i.e. parts that are detected as surface but are not. Finally, the surface itself might cause trouble if it is highly tortuous, which led to the introduction of the parameter of surface regularity *Reg_{surf}*.

Table 2. Image parameters.

Image characteristics	Label	Description	Calculation	Aspect for normalized values	
				1.0	5.0
Flame – propellant contrast	<i>Cont</i>	Difference between average signal levels for the gas area and solid propellant area	average $S(\text{gas})$ - average $S(\text{propellant})$	Low contrast	Clear contrast
Flame – surface border gradient	<i>Grad</i>	Gradient at the border of the propellant surface	dS / dy	Smooth gradient	Sharp gradient
Flame homogeneity	<i>Hom</i>	Homogeneity of the flame area	Standard deviation for $S(\text{gas})$	Objects and smoke above the surface	Uniform area above the surface
Surface regularity	<i>Reg_{surf}</i>	If the surface is flat overall or prone to ample patterns	Surface length	Uneven and curved surface	Quasi-planar surface

As an illustration of the range of image conditions, a sample image is presented for each of the six analyzed series in Figure 3. As an indication of the image parameters, radar plots are included showing the 4 image characteristics rated on a normalized scale from 1 to 5 (1 corresponding to difficult conditions with large error levels). The normalized scale was obtained by evaluating the 4 characteristics for all analyzed images, rating the worst value as 1.0 and the best as 5.0, and applying a linear scale for the intermediates values. The formula for each parameter are gathered in Table 2 with the signal intensity level labelled as S .

The three propellant compositions with inert particles were tested at 1.0 MPa, leading to clear image conditions only differentiated by the size of single particles and aggregates. The glass-seeded propellant was also tested at 3.0 MPa, e.g. leading to heterogeneous gas conditions. Finally, the aluminum-seeded composition led to much more complex images in the gas area where bright burning droplets were surrounded by smokes and sharp gas gradients; it was tested at 2.0 and 3.0 MPa. Overall, as intended, surface was studied for six very different image conditions.

3. Surface analysis approach

The present section introduces the image analyses that were applied in order to investigate propellant-surface phenomena on shadowgraphy images.

3.1. Active contour method

Active contour methods have been introduced in the late 80’s [20] and have become a classical framework for curve and object detection in image. Active contour are regular non parametric curves aimed at fitting borders between regions within an image. The goal is to be flexible enough to detect a wide range of shapes without being unstable under high noise levels. For the latter requirement, active contours include a regularization process. For example, several methods in the line of [20] define the contour as the minimizer of a two-term energy formula combining an “external energy” associated to the fact that the contour passes onto strong image gradients and an “internal energy” limiting large changes in the curvature. In the present work, we use the more recent approach of [21] where the external term favours the segmentation, by the contour, of two regions with contrasted levels, while the regularization of the curve is obtained by minimizing its length. This segmentation-based approach has been shown

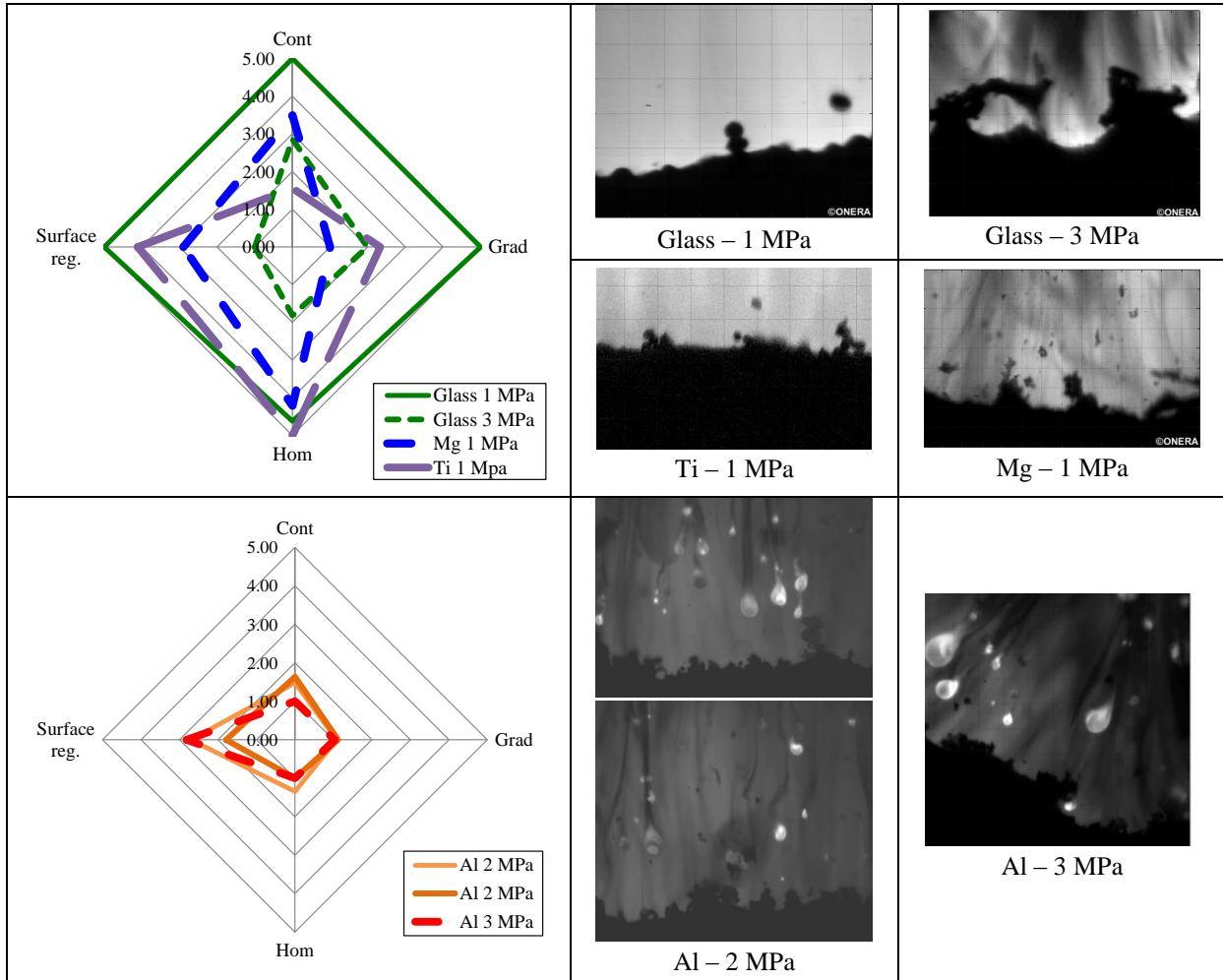


Figure 3. Examples of shadowgraphy images with their image characteristic displayed on radar graphs.

to be less sensitive to the noise level and to the variations of the gradient strength along the border, both points being of interest considering our images.

In order to illustrate its performance for propellant surface study, the active contour method was compared to a fixed threshold approach, which is certainly the most intuitive approach used to divide images into two regions with very contrasted signal levels (e.g. a dark area and a bright one). In the case of shadowgraphy experiments with the present set-up, a test series typically includes from 500 to 5000 individual images, hence a fixed threshold cannot be set for each individual image. This can lead to issues associated with shot noise or drifting image conditions during combustion. Using a fixed threshold is both a simple but limited approach for extensive surface evaluation; it is a good baseline method to evaluate the chosen active contour method. In the following, the baseline method will be labeled “fixed threshold”, and the tested method is labelled “active contour”.

3.2. Evaluation of the surface detection

Performances are evaluated compared to ground truth (GT) for sample images, e.g. by delimitating manually the propellant surface location for some test images. This manual reference is labelled “GT”. Each point located on a detected surface is compared to GT: if the location matches the GT, the point is a “True Positive” (*TP*), whereas a location that does not match GT is a “False Positive” (i.e. an erroneous point on the detected contour). The quality of detection is then evaluated in terms of Precision (*Pr*) and Recall (*Rec*). Precision evaluates the proportion of surface detection that is good, or *TP*. Recall evaluates the proportion of GT that is effectively detected. The formula for *Pr* and *Rec* and presented below (equation (1)).

$$\begin{aligned} \text{Pr} &= \frac{TP}{TP + FP} \\ \text{Rec} &= \frac{TP}{GT} \end{aligned} \quad (1)$$

Obviously, the GT is itself prone to errors since it is defined manually by the operator. Hence the *TP* condition was not defined as a perfect pixel-to-pixel match between the detected point on the profile and GT. Various levels of tolerance were introduced to quantify the closeness to GT. This is illustrated for a portion of GT on Figure 6 a). The white stripe corresponds to $GT \pm 3$ pix and various tolerance levels are displayed in grayscale from ± 5 pix to ± 80 pix. Hence a given detected surface will be compared to this tolerance map, as shown with the example on Figure 6 b). Most parts of the detected surface in blue remains within the white stripe and is considered as *TP* within a tolerance of 3 pix. A small portion of surface, designated by a red circle, is found further than 3 pixels from GT and is then *FP* within the 3 pixel tolerance. In the present paper, Precision and Recall have both been calculated within a ± 3 pix interval. But larger tolerance levels have also been used in order to study portion of detected surface far away from GT: proportion of detected surface further than 10, 15, 20 pixels away from GT...

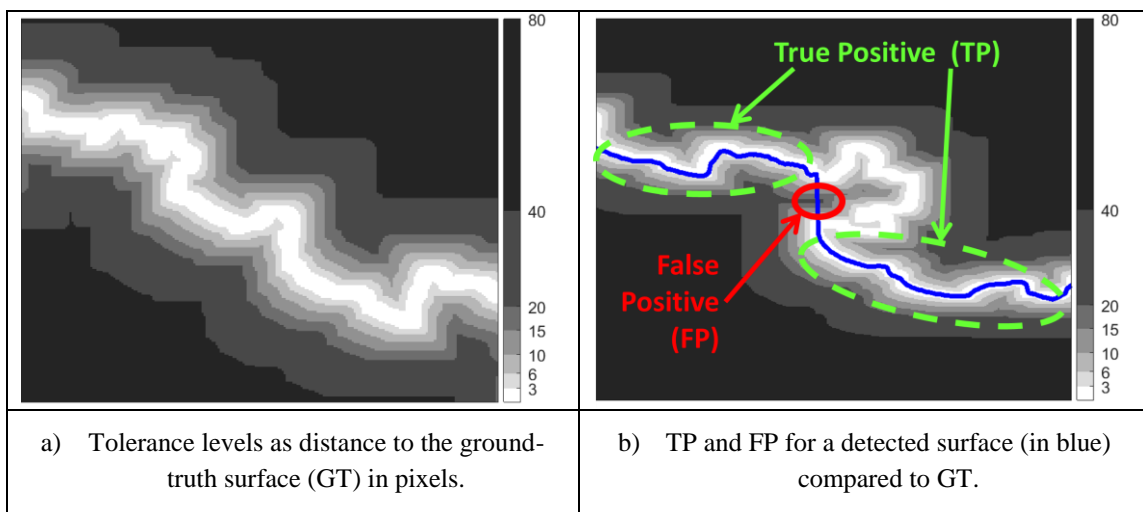


Figure 4. Tolerance levels regarding GT and associated scores as TP and FP for a given surface detection.

3.3. Pattern of interest on the surface

Assuming that the propellant surface is well detected, its shape is analyzed in order to study the physical phenomena that are taking place. As the focus of the present work is mostly to improve aluminum-agglomeration study, it is interesting to detect coral-like shapes that would show agglomeration processes on the surface before and during aluminum melting. The detection is similar to the selection of key points on shapes, an important step for some methods of shape recognition. An approach based on surface curvature was defined, inspired by the work of Mokhtarian et al. [22]. The contour of the surface is defined as coordinates $x(t)$ and $y(t)$, where t is a curvilinear abscissa. The curvature κ is obtained from the first and second derivative of the coordinates x and y , labelled with single and double dots (\dot{x} and \ddot{x} for x for instance). The formula for κ is the following:

$$\kappa = \frac{\dot{x}\ddot{y} - \dot{y}\ddot{x}}{(\dot{x}^2 + \dot{y}^2)^{1.5}} \quad (2)$$

The curvature is used as the main criterion to detect a protruding portion of the propellant surface. However, studying the curvature of a fully detailed surface will lead to several local maxima and a high noise level, making it difficult to discriminate between strong relevant curvature peaks and minor profile fluctuations. Hence, we conduct a multiscale analysis in the line of [23], using numerical Gaussian filtering of the contour so as to increase contrast for larger shapes. Filtering is obtained by convolution of $x(t)$ and $y(t)$ with a one dimensional Gaussian kernel of width σ , $g(t, \sigma)$:

$$g(t, \sigma) = \frac{1}{\sigma\sqrt{2\pi}} e^{-\frac{t^2}{2\sigma^2}} \quad (3)$$

Various filtering scales are used, e.g. several values of σ . This is a way to classify the detected shapes of interest as a function of size; as shown with Figure 5 for two protruding objects. On the left-hand side, part a single particle is emerging from the surface, whereas a small string of 3 particles is visible on the right-hand side. In both cases, 3 numerical filters are applied with increasing σ from filter #1 to #3, leading to smoother and smoother filtered contours, as revealed by the curvature plots below. In the case of the isolated emerging particle, a clear curvature maximum is only visible for filter #1, whereas it can be clearly seen for filter #1 and #2 for the 3-particle string. Such multiscale curvature analysis is a convenient way to classify protruding objects without any other analysis. A set of thresholds for curvature maximum value was defined for each filter sizes as a criterion to extract shapes along the propellant surface. The location of curvature minima on each side of the detected shape was used as the limits of the extracted shape.

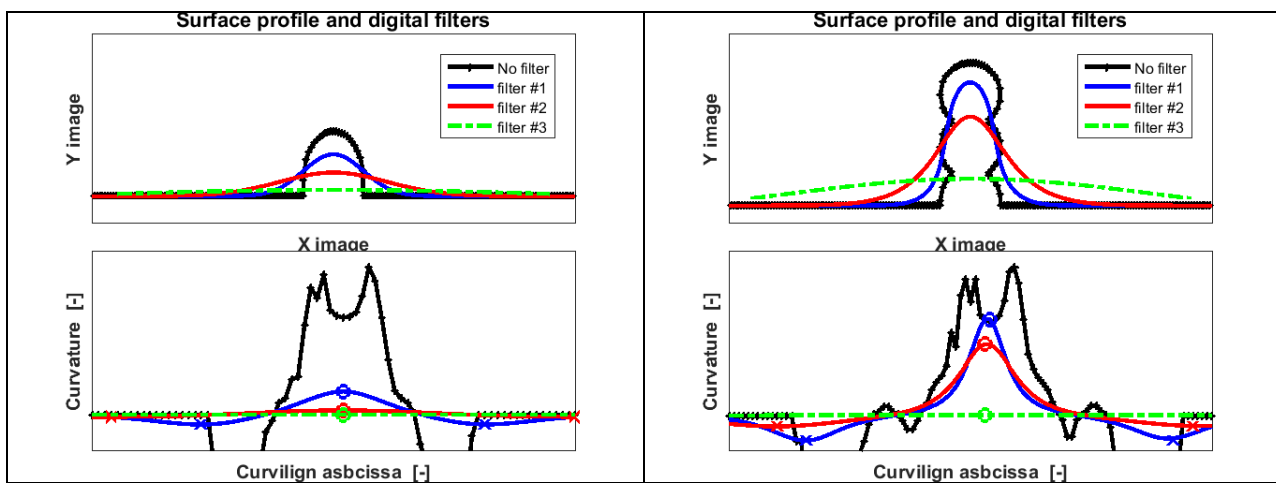


Figure 5. Curvature of object on the surface for various filter sizes.

Top graphs: Surface profiles without and after various filtering (increasing σ from filter #1 to #3).

Bottom graph: associated curvature.

The detected objects have been analyzed in terms on their lifetime on the surface as well as their apparent area. A same object is indeed usually seen on several images before it leaves the surface, so shapes on successive images have been associated as the same object based on criteria for their maximum curvature and extremal points. This provided a first evaluation of the lifetime on the surface of agglomeration patterns, limited to shapes that do not vary a lot over time since the association criteria remain crude. The protruding portion of the shape above the surface was used to evaluate the size of detected objects with an equivalent diameter calculated from the apparent area. Size distribution were calculated from all the detected objects and compared to the diameter distribution for the single particles that were seeded into the propellant (obtained from a laser granulometer before propellant preparation).

4. Results

4.1. Quality of surface detection with the active contour method

Figure 6 shows the propellant surfaces detected by the two tested methods as well as GT, for two test conditions. The left-hand side picture corresponds to combustion for propellant “glass” at initial pressure 1 MPa, which is the most favorable condition that was tested, as shown with radar plot from Figure 4. Both detection methods follow GT, even for the protruding snowman-like shape; the fixed threshold surface only has issues detecting the concave portions in this vertical shape. The right-hand side of Figure 6 displays propellant surface for the aluminized propellant at 3 MPa, one the most difficult image conditions for surface detection tested here. The active contour method remains close to GT, whereas the fixed threshold method is sometimes far away from GT, particularly for a complex shape at the center of the image. This first qualitative comparison shows that the fixed threshold method might not be as

robust as the active contour approach for more complex conditions, as expected. Figure 7 presents portions of the same two surfaces in terms of distance to GT. This clearly shows that the active contour method remains within the tolerance interval of ± 3 pix, whereas the fixed threshold approach can lead to portions further than 10 to 20 pixels from GT. Precision remains high for the active contour approach but it can drop with image conditions for a fixed threshold evaluation.

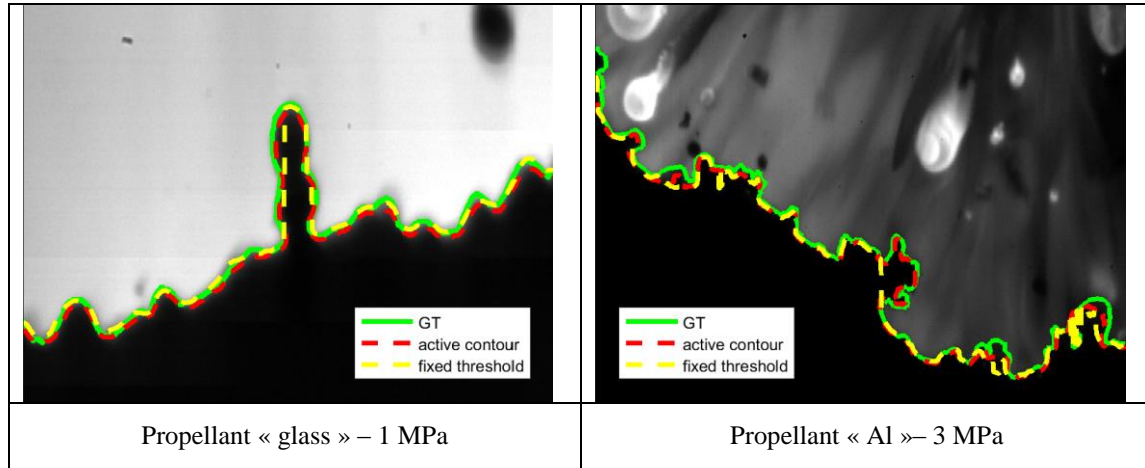


Figure 6. GT propellant surface and detected surfaces for the two analysis methods.

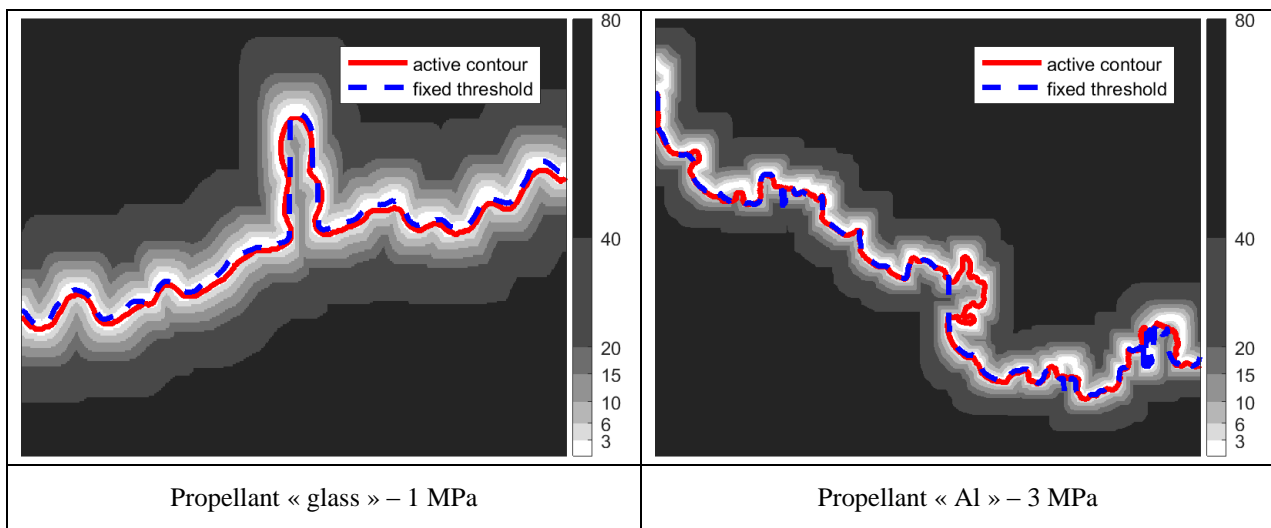


Figure 7. Propellant surface detection compared to GT for the two analysis methods (fixed threshold in blue dash, active contour in red). Gray scale corresponds to distance to ground truth in pixels.

Precision and Recall values are plotted in Figure 8 and Figure 9. In both figures, Recall and Precision are displayed for the two detection approaches, plotted as a function of the 4 images characteristics (Contrast, border gradient, surface regularity, homogeneity). Figure 8 demonstrates that, in fact, Precision is quite similar for the two detection approaches: in the end, along full image width, the detected propellant surfaces remain close to GT, be it from a fixed threshold approach or the active contour method. As expected, Precision is close to 100% when image characteristics are more favorable (i.e. close to 5.0) in the case propellant “glass” at 1.0 MPa. Precision shows no real dependence to propellant / flame contrast nor gas-area homogeneity, but a stronger dependence to flame / propellant gradient levels and surface regularity. The last two image characteristics were the most constraining parameter for surface detection in the tested image sets.

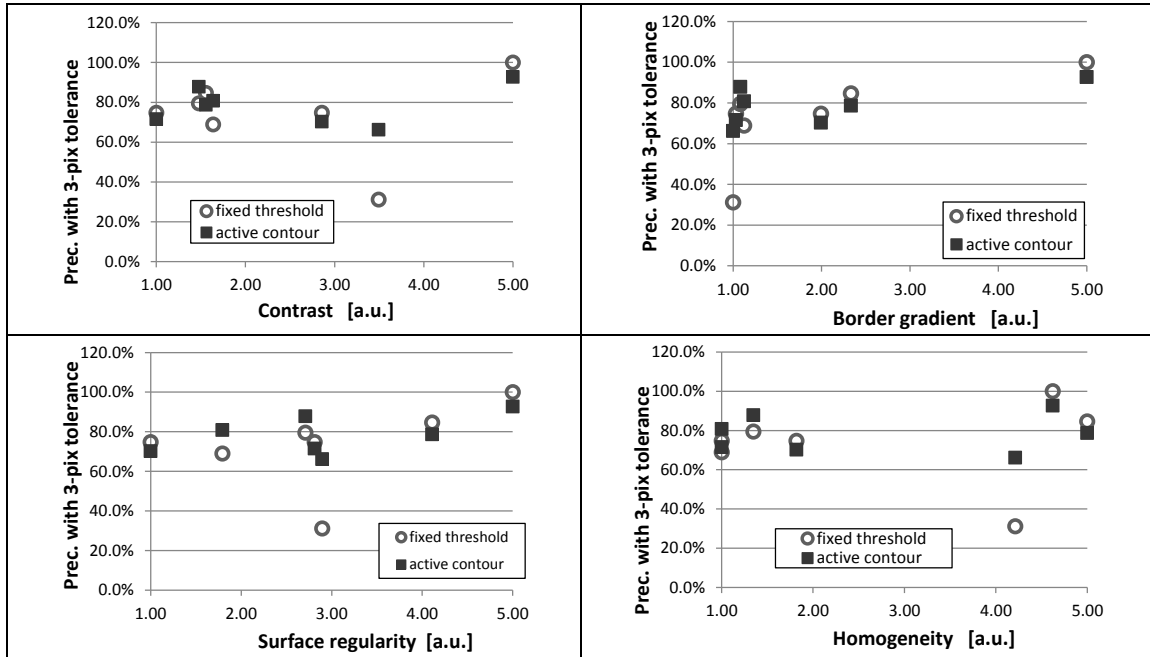


Figure 8. Precision as a function of the 4 image characteristics. Plots for the two surface-detection methods.

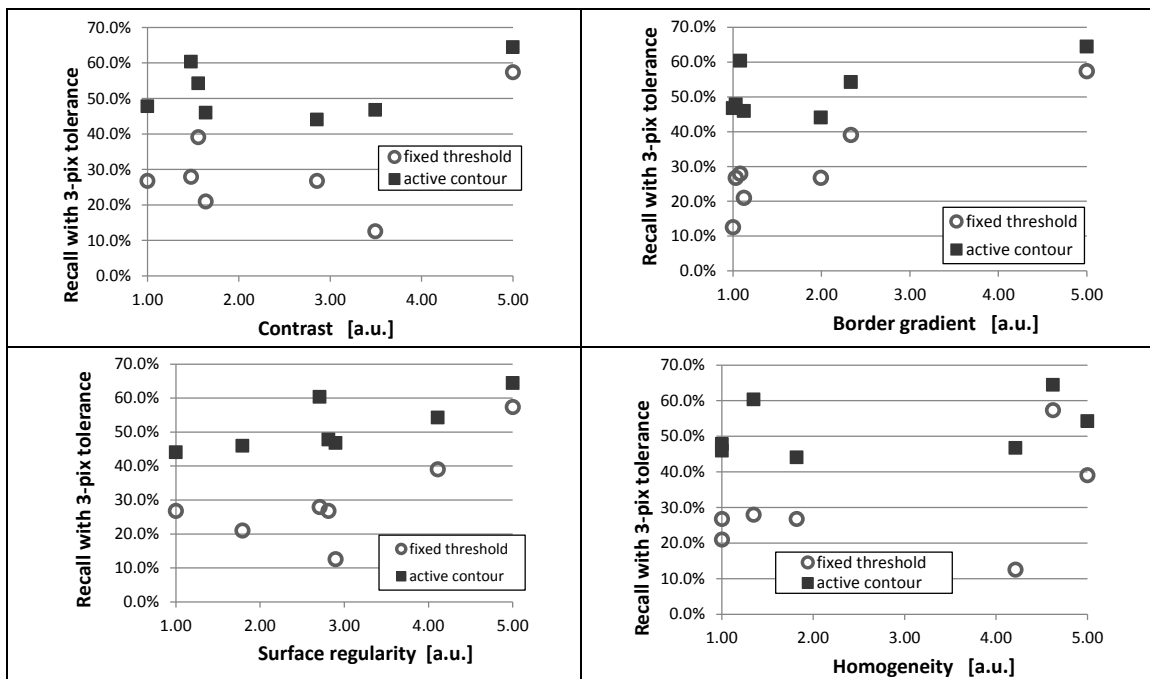


Figure 9. Recall as a function of the 4 image characteristics. Plots for the two surface-detection methods.

However, there is a greater discrepancy between the two methods regarding Recall, e.g. regarding their capacity to perfectly recover the exact propellant surface as specified via GT. For all conditions, *Rec* value for the active contour method is significantly larger than for a fixed threshold approach. Moreover, the *Rec* deterioration with harsher flame / surface gradient and surface regularity is much more pronounced with a fixed threshold detection: it is reduced from 60 to 10% in that case whereas results for the active contour method are only deteriorated from 65% to 45%. It illustrates the stronger robustness of the active contour method in harsh conditions. It is an interesting feature since image conditions depend strongly on measurement conditions, such as propellant composition, aluminum-particle initial size distributions, operating pressure...

More generally, low Recall levels on surface detections are particularly negative when detecting specific shapes is the main objective. The issue was obvious for propellant "Al" in Figure 7 where the fixed threshold method by-

passed a complex protruding portion – surface phenomena associated to this surface feature would not be studied in this case. Recall values commented previously correspond to values integrated along the full surface and work in a binary way (either a portion of GT is recalled within the 3-pixel tolerance or not) but it does not show how far the detected surface is from the missed GT portion. Plots from Figure 10 shows the proportion of the detected surface that is further than a certain distance from GT, plotted as 1 – cumulated probability: for instance, for the abscissa value “6 pixels”, the graphs corresponds to the proportion of detected surface further than 6 pixels to GT. In the case of the propellant “glass”, no part of the fixed threshold surface is found further than 3 pixels to GT: the detected surface is consistent with GT. But in the case of the harsh conditions associated to the aluminized propellant at 3 MPa, 12% of the propellant surface detected via fixed threshold is in fact further than 6 pixels to GT. In this case, it seems highly probable that several significant shapes of interest have been missed partially or completely by-passed. The plot shows that the active contour method remain much closer to GT, with almost no portion of the detected surface found 10 pixels away from GT. The method is more reliable over a large range of conditions than a basic fixed threshold approach and is well-suited for quantitative analysis of surface phenomena.

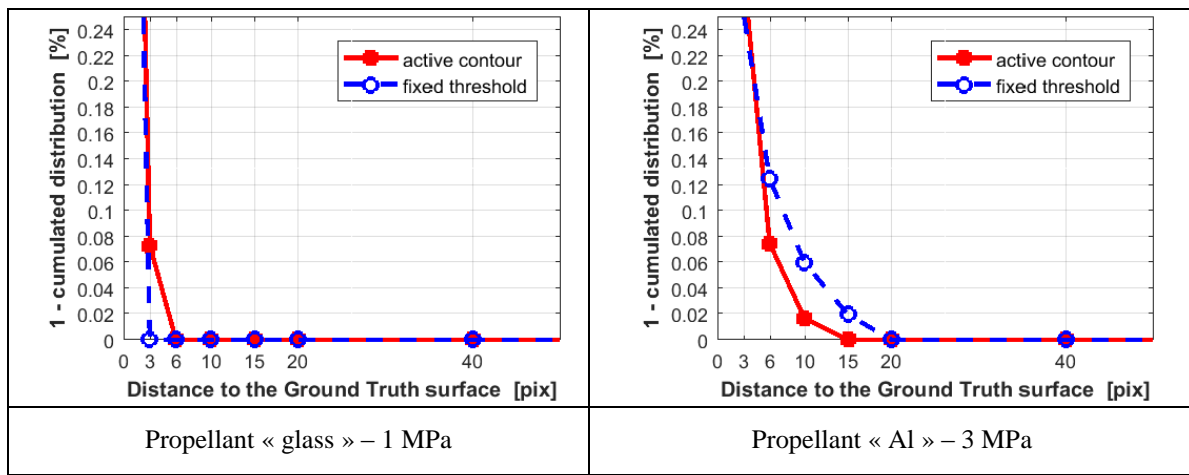


Figure 10. Proportion of the detected surface as a function of the distance to GT. Plots as 1 – cumulated probability.

4.2. Detection of shapes of interest on the propellant surface

The curvature-based analysis presented earlier is efficient to detect select specific portions of interest on the surface as presented with Figure 11 to Figure 13 for various image conditions. First, Figure 11 demonstrates the approach for the favorable conditions with propellant “Glass”: a small protruding particle is first visible on the surface, then is associated with a second one, and the shape remains on the surface more than 40 successive image, i.e. more than 10 ms. The method is also able to follow shapes that varies more along time, as shown for propellant “Mg” (Figure 12). A small protrusion is first detected but then evolves to a tree-like shape with two branches (image #22) that finally collapses closer to the surface (image #32). Following a shape that morphs is a necessary feature to study precisely aggregation, melting, and final agglomerate ejection. The present detected shape shows the promising capacity of the method. Still, improvements remain required since shape variations can be complex, as illustrated with Figure 13 for the aluminized propellant. In this case, a protruding shape appears on the surface and remains visible until the burning Al droplet leaves the surface. Small shapes are detected under the droplet after it leaves, showing that the method needs to be refined to take into account surface ejection more efficiently. This will imply connecting surface analysis to object detections right above the surface.

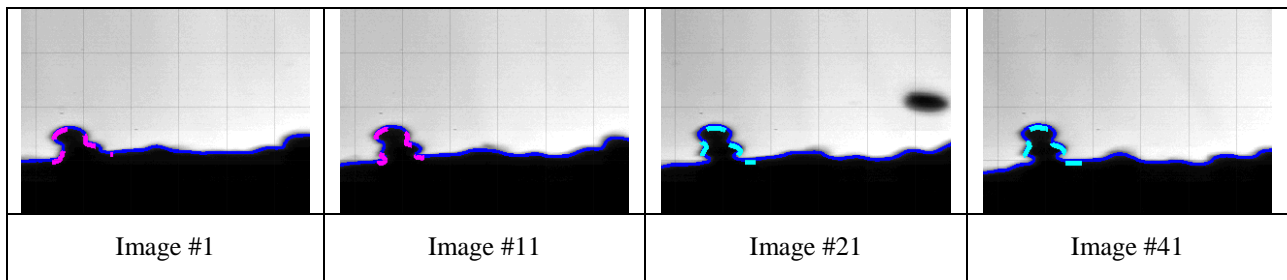


Figure 11. Example of detected shape on successive images. Propellant « Glass » at 1 MPa.

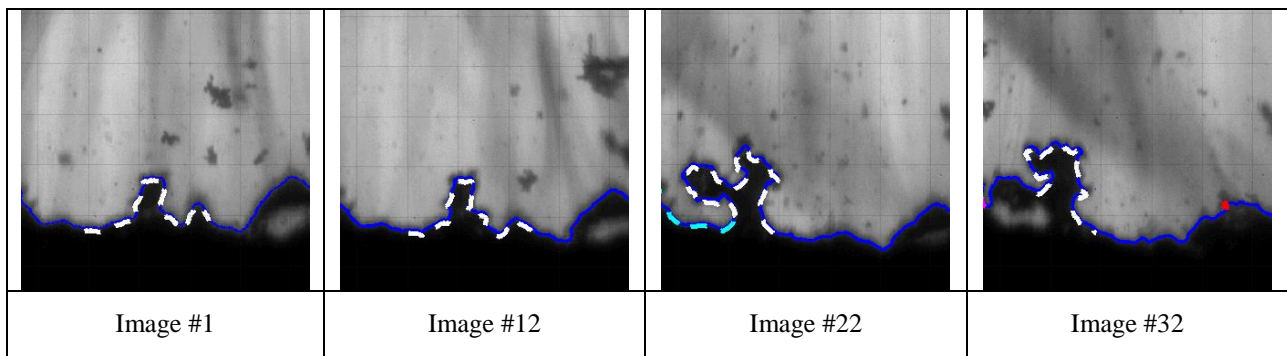


Figure 12. Example of a detected object on successive images. Propellant « Mg » at 1 MPa.

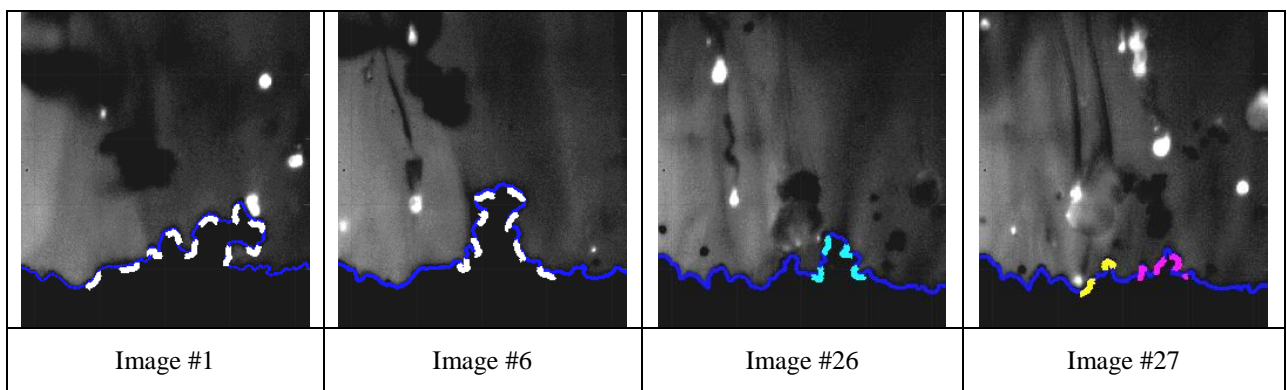


Figure 13. Example of detected shape on successive images. Propellant « Al » at 2 MPa.

But even with remaining adjustments, the detection of shape on the surface makes it possible to access interesting quantitative analysis of surface phenomena. Figure 14 shows size distributions for the detected shapes, compared to diameter distribution of the initial single particles seeded into the propellant. Graphs correspond to the propellant “Ti” at 1 MPa and the two tested pressures for the aluminized propellant. The size distributions for the surface objects are shifted to larger diameter compared to the single-particle distributions, which seems consistent with agglomeration phenomena involving two or more single particles. It is also interesting to notice that surface shapes seem slightly larger at 2.0 MPa than 3.0 MPa for the aluminum propellant, which is consistent with the usual reduction of agglomeration phenomena with increasing operating pressure.

Figure 15 overlaps graphs for two kinds of particles, Al and TiO_2 , in order to show that the evaluated size distributions do vary with composition and do not correspond to mere analysis bias. The size distributions from Figure 15 clearly show diameter intervals that are significantly different for the two particle compositions. Similarly, lifetime cumulated distributions suggest different surface behaviors depending on the particle composition as well as the operating pressure: surface shapes remains on the surface for a shorter time at 3.0 MPa, which is expected considering the increase in surface regression rate with pressure. The first results are promising for future

quantitative study of the agglomeration phenomena and combustion phenomena taking place on the propellant surface before ejection of the aluminum burning droplets.

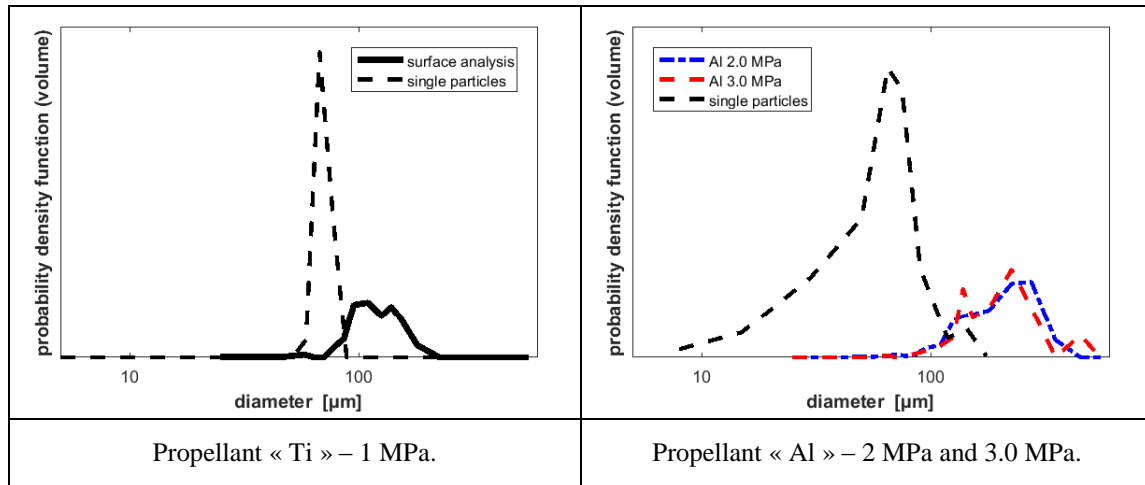


Figure 14. Probability distribution in volume compared to single-particle distribution.

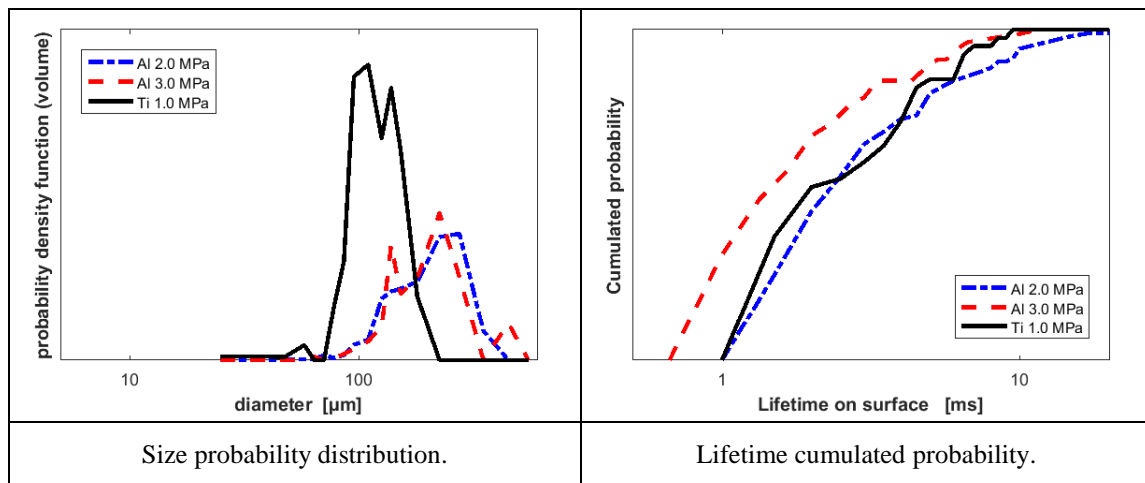


Figure 15. Analysis of detected surface shapes in terms of size and lifetime distribution. Detection for propellant “Ti” at 1.0 MPa and propellant “Al” and 2.0 and 3.0 MPa.

5. Conclusion & perspectives

Present work has shown an image processing approach used to study propellant surface during combustion in order to improve understanding on aluminum-agglomeration phenomena. The method is based on the analysis of shadowgraphy images acquired during combustion measurements. An active contour approach is applied to the images in order to extract propellant surface border and curvature criteria are applied to the surface for various level of numerical filtering in order to select shapes of interest that can be followed in time over various images. This gives access to size distribution and surface lifetime distribution for the shape. The method was applied to 6 test images obtained via combustion of 4 test propellants seeded with inert particles or aluminum particles; the 6 tests corresponded to a wide range of images conditions of increasing complexity. The active contour demonstrated good levels of performance compared to GT surface and an interesting robustness for the tested image conditions. Various kinds of shapes were detected and followed over up 40 successive images and more. Size distributions and lifetime distributions were analyzed and suggested that quantitative data on surface phenomena should be accessible via the image analysis method.

Improvements still need to be made to incorporate particle ejection from the surface to lifetime studies. But the method is highly promising to support agglomeration modelling and simulations. Access to lifetime and aggregate size should be highly valuable as input data for more details surface models associated to agglomeration. The resulting statistics should also be available as validation data for heterogeneous combustion simulations based on packing approaches. All this experimental data analysis should help developing more complete predictions approaches to predict aluminum agglomeration more accurately, a crucial aspects for better simulation of two-phase flows in solid-rocket motor.

Symbols and abbreviations

AP	Ammonium Perchlorate	Pr	Precision
Cont	Flame / propellant contrast	Rec	Recal
FP	False Positive	Regsurf	Surface regularity
Grad	Flame / surface gradient	σ	Width of Gaussian kernel
GT	Ground Truth	S	Signal intensity level
Hom	Flame homogeneity	t	Curvi-linear coordinate
HTPB	hydroxyl-terminated polybutadiene	TP	True Positive
κ	Surface curvature	x(t), y(t)	Surface coordinates

Acknowledgments

We acknowledge the financial support of CNES for the development of present shadowgraphy analysis.

References

- [1] Guéry, J.F., Ballereau, S., Godfroy, F., Gallier, S., Orlandi, O., Della Pietra, P., Robert, E. & Cesco, N. (2008). Thrust Oscillations in Solid Motors. In Proc. 44th AIAA 2008-4979
- [2] S. Gallier, F. Godfroy (2009). Aluminum Combustion Driven Instabilities in Solid Rocket Motors. *Journal of Propulsion and Power*, Vol. 25, No. 2.
- [3] Casalis, G., Boyer & G., Radenac, E. (2011). Some recent advances in the instabilities occurring in long Solid Rocket Motors. In Proc. 47th AIAA 2011-5642.
- [4] Willoughby P. G., Baker K.L.n Hermsen R.W. (1971) Photographic study of solid propellant burning in an acceleration environment, 13th International Symposium on Combustion, 9-13 May 1971, Pittsburgh
- [5] Salita M. 1994. Survey of recent Al₂O₃ droplet size data in solid rocket chambers, nozzles and plumes, 31st JANNAF Combustion Meeting, 17-21 October 1994, Sunnyvale
- [6] Trubert J.F. 2000. Agglomeration and combustion of aluminium particles in solid rocket motors. 2nd European Conference on Launcher Technology, Space Solid Propulsion, Paper 44
- [7] Beckstead M.W. 1977. A model for solid propellant combustion, *Proceedings of the 14th JANNAF Combustion Meeting*, CPIA Pub. 292, Vol. 1, Johns Hopkins University, Baltimore, Maryland, USA, pp. 281-306
- [8] Grigoriev V.G. Kutsenogii K.P., Zarko V.E. 1981. Model of Aluminum agglomeration during the combustion of a composite propellant, *Comb. Expl. Shock Waves*, vol. 17, p. 356
- [9] Cohen, N.S. 1983. A pocket model for aluminium agglomeration in composite propellants, *AIAA Journal*, Vol. 21, No. 5.
- [10] Gallier. S. 2009. A stochastic pocket model for aluminum agglomeration in solid propellants. *Propellants Explos. Pyrotech.*, Vol. 34(2), pp. 97-105.
- [11] Yavor, Y., Gany, A. & Beckstead, M.W. 2014. Modeling of the agglomeration phenomena in combustion of aluminized composite solid propellant. *Propellants Explos. Pyrotech.*, Vol. 39, pp. 108-116.
- [12] Maggi F. & DeLuca, L.T. 2015. Pocket model for aluminium agglomeration based in propellant microstructure. *AIAA Journal*, Vol. 53, No. 11, pp. 3395-3403.
- [13] DeLuca L.T., Paravan C., Reina A. Marchesi E. Maggi F. Bandera A., Colombo G. 2010. Aggregation and incipient agglomeration in metallized solid propellants and solid fuels for rocket propulsion, 48th AIAA/ASME/SAE/ASEE Joint Propulsion Conference & Exhibit, 26-28 July 2010, Nashville, TN.

- [14] Mullen J.C., Brewster M. Q. 2011. Reduced agglomeration of aluminum in wide-distribution composite propellants, *Journal of Propulsion and Power*, Vol. 27, No. 3, pp. 650-661
- [15] Sippel T.R., Son S. F., Groven L.J. 2014. Aluminum agglomeration reduction in a composite propellant using tailored Al/PTFE particles, *Combustion and Flame*. 161:311-321
- [16] Cauty, F. & Erades, C. 2012. Tracking of aluminum particles burning in solid propellant combustion gases by focusing schlieren technique. *In Proc. 15th International Symposium on Flow Visualization*.
- [17] Devillers R.W., C. Erades, D. Lambert, J. Belessa. 2014. Mesure et suivi de particules, agglomérats et gouttes en combustion au-dessus de la surface d'un propergol en combustion. *14th CFTL*, Marseille.
- [18] Nugue, M., R. W. Devillers, G. Le Besnerais, N. Cesco. 2016. Particle detection & size evaluation in solid propellant flames via experimental image analysis to improve two-phase flow simulation in rocket motors. *Space Propulsion conference*.
- [19] Weinstein, L. 1993. Large-field high-brightness focusing Schlieren system, *AIAA Journal*. 31:7: 1250-1255
- [20] Kass, M., A. Witkin, D. Terzopoulos. 1988, Snakes: active contour models, *International Journal of Computer Vision*. 321-331
- [21] Chan, T.F., L. A. Vese. 2001. Active contours without edges. *IEEE transactions on image processing*, Vol. 10, No 2.
- [22] Mokhtarian, F., A. Mackworth, Scale-based description and recognition of planar curves and two-dimensional shapes, *IEEE Transactions on pattern analysis and machine intelligence*, vol. PAMI-8, No 1, (1986)
- [23] Lindeberg, T. 2013. Scale-space theory in computer vision. Springer Science & Business Media.